International Journal of Pharmaceutics 672 (2025) 125326

Contents lists available at ScienceDirect

International Journal of Pharmaceutics

journal homepage: www.elsevier.com/locate/ijpharm

Nitroreductase-responsive gated mesoporous silica nanocarriers for hypoxia-targeted drug delivery

Mariana Barros [a], José A. Sáez [a,b], Pau Arroyo [a,b], J. Vicente Ros-Lis [a], M. Dolores Garrido [c], Ramón Martínez-Máñez [a,d,e,f,g], M. Carmen Terencio [a,h], M. Carmen Montesinos [a,h], Pablo Gaviña [a,b,e,*]

[a] Instituto Interuniversitario de Investigación de Reconocimiento Molecular y Desarrollo Tecnológico (IDM), Universitat de Valencia - Universitat Politècnica de València, C/ Doctor Moliner, 50, Burjassot 46100, Valencia, Spain
[b] Departamento de Química Orgánica, Universitat de València, C/ Doctor Moliner 50 46100, Burjassot, Valencia, Spain
[c] Institut de Ciència dels Materials (ICMUV), Universitat de València, C/ Catedrático José Beltrán 2, Paterna 46980, Valencia, Spain
[d] Departamento de Química, Universitat Politècnica de València, Camino de Vera s/n 46022, Valencia, Spain
[e] CIBER de Bioingeniería, Biomateriales y Nanomedicina (CIBER-BBN), Instituto de Salud Carlos III, Spain
[f] Unidad Mixta UPV-CIPF de Investigación en Mecanismos de Enfermedades y Nanomedicina, Universitat Politècnica de València, Centro de Investigación Príncipe Felipe, C/ Eduardo Primo Yúfera 3 46100, Valencia, Spain
[g] Unidad Mixta de Investigación en Nanomedicina y Sensores, Universitat Politècnica de València, Instituto de Investigación Sanitaria La Fe, Av Fernando Abril Martorell 106 46026, Valencia, Spain
[h] Departamento de Farmacología, Universitat de València, Av. Vicent Andrés Estellés s/n, Burjassot 46100, Valencia, Spain

ARTICLE INFO

Keywords:
Hypoxia-responsive
Nitroreductase
Doxorubicin
Controlled delivery
Mesoporous silica nanocarriers
Self-immolative gatekeepers

ABSTRACT

Hypoxia, *i.e.*, low oxygen concentration at the tissue level, is a common feature of most solid tumors, and is responsible for their enhanced aggressiveness and resistance to chemotherapy, radiotherapy and photodynamic therapy. Hypoxic microenvironments are also characterized by the overexpression of various reductase enzymes such as nitroreductases. Herein, we report a hypoxia-responsive hybrid nanomaterial consisting of mesoporous silica nanoparticles, loaded with the chemotherapy drug doxorubicin, and functionalized on their surface with a self-immolative gatekeeper responsive to nitroreductases, for the controlled release of the cargo. Thus, under bioreductive conditions, elicited by the presence of nitroreductase and NADH, the reduction of the nitroaromatic containing molecular gate induces a self-immolative elimination leading to the disintegration of the gatekeeper and the delivery of the doxorubicin from inside the pores. The nitroreductase-responsive nanocarrier has been tested *in vitro* with A549 cells, that are known to express nitroreductase, to demonstrate its effectiveness as drug carrier for doxorubicin release, showing great potential for the treatment of hypoxic tumors.

1. Introduction

According to the World Health Organization (WHO), cancer is a leading cause of death all over the world. (Cancer Tomorrow. International Agency for Research on Cancer, WHO, n.d.) Malignant cells cause biological and genetic changes that affect tissue cells, causing them to grow uncontrollably. Most tumors grow as abnormal masses of tissue (i.e. solid tumors that account for 90 % of human cancers), (Ng et al., 2023) and a situation that manifests most of them is hypoxia, which is a low oxygen concentration (pO_2 values $\leq$ 2.5 mmHg). (Vaupel and Mayer, 2007) This is due to the inadequate blood supply inside of the tumor because of the dysfunctional tumor vasculature, which does not allow the metabolic oxygen demand of the tumor cells to be met. (Elmes, 2016; Siemann and Horsman, 2015).

Cancer treatments encompass both invasive techniques, such as surgery, and non-invasive methods like radiotherapy, chemotherapy or photodynamic therapy. (Debela et al., 2021) However, these traditional therapies are often unsatisfactory due to side effects as some of them are non-specific and affect healthy cells. (Mousa and Bharali, 2011) Moreover, hypoxic cells resist conventional radiotherapy and chemotherapy treatments. (Hompland et al., 2021; Graham and Unger, 2018) For instance hypoxic tumor cells require to be eradicated three to five times higher X-ray dosage compared with tumor cells in properly oxygenated conditions. (Zdrowowicz et al., 2022; Sørensen and Horsman, 2020)

* Corresponding author.
E-mail address: pablo.gavina@uv.es (P. Gaviña).

https://doi.org/10.1016/j.ijpharm.2025.125326
Received 29 November 2024; Received in revised form 4 February 2025; Accepted 6 February 2025
Available online 13 February 2025

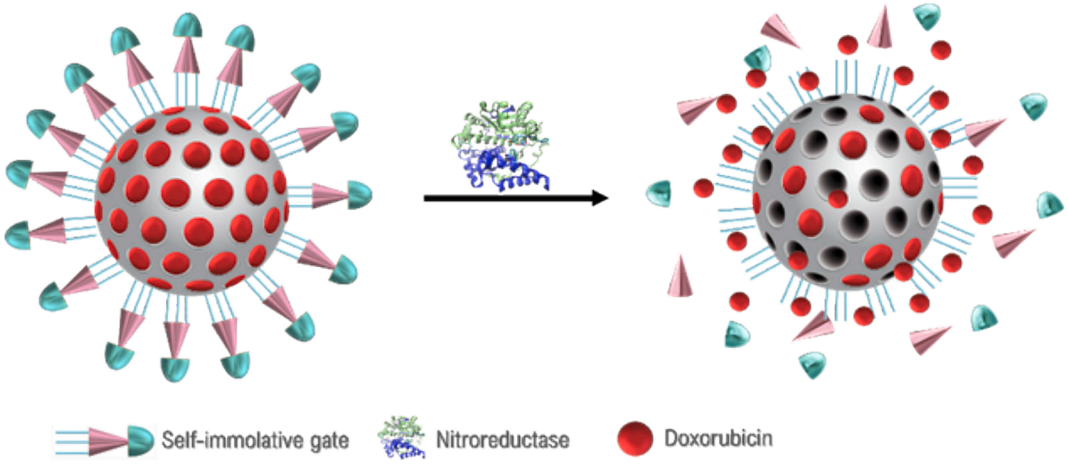

Fig. 1. Drug delivery strategy for targeting hypoxic tumors, based on nitroreductase-responsive gated mesoporous silica nanocarriers.

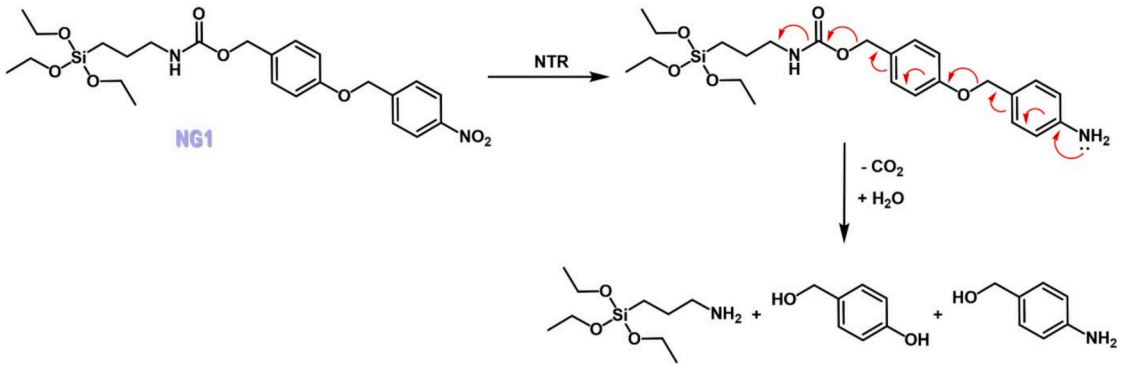

Scheme 1. Structure of the synthesized molecular gate **NG1**, and self-immolative process after the reduction of the nitro group to amine in the presence of NTR.

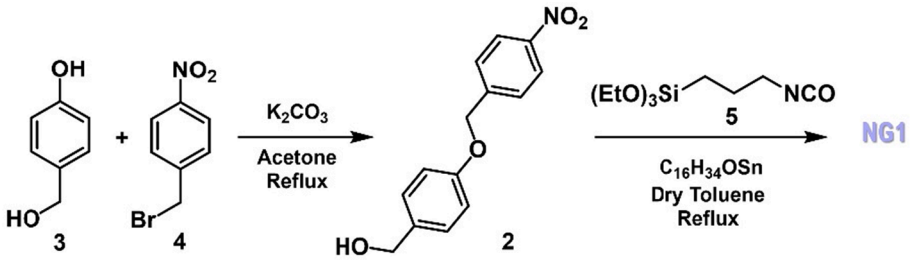

Scheme 2. Synthesis of the nitro gatekeeper **NG1**.

Also, hypoxic cells are more resistant to anticancer drugs. One reason for this is that hypoxic cells divide more slowly than normal because they are in a low-oxygen environment and most antitumor drugs are effective against highly proliferating cells. Besides, hypoxic cells are far from the blood vessels through which the drugs are delivered. (Minassian et al., 2019).

Understanding cancer biology can lead to better diagnosis and treatment methods, and several advances have been made in this field in recent decades. It is well known that hypoxic microenvironment is a reducing medium containing a high concentration of reductase enzymes, such as nitroreductases (NTR), azoreductases, or DT-diaphorases, which can reduce nitro and azo groups, and quinones in the presence of NADH or NADPH. (Elmes, 2016; Fang et al., 2018) Given the resistance of hypoxic cells to conventional treatments, the development of nanomedicines has been proposed to overcome this resistance by taking advantage of these particular biological conditions. In this sense, one of the strategies proposed is to use controlled drug release systems under hypoxic conditions. Reductase enzymes may provide a controlled release mechanism via the design of nanomaterials in which the reduction of selected organic moieties allow delivery of a drug. (Thambi et al., 2014; Kumari et al., 2020; Zhou et al., 2020; Yan et al., 2019; Li et al., 2020).

Among different nanoparticles, mesoporous silica nanoparticles (MSNs) are good candidates for drug delivery applications due to their excellent biocompatibility, high loading capacity, and easy surface functionalization. (Xu et al., 2022; Wang et al., 2021; Ye et al., 2025) Moreover, MSNs can be equipped with molecular gates (also known as gatekeepers or nanovalves) that cap the pores and allow controlled drug delivery in the presence of physical, chemical or biochemical stimuli. (Aznar et al., 2016) Considering the very few existing studies on mesoporous silica nanoparticles (MSNs) for controlled drug release in hypoxic tumors, (Lee et al., 2017; Khatoon et al., 2018) we report herein the

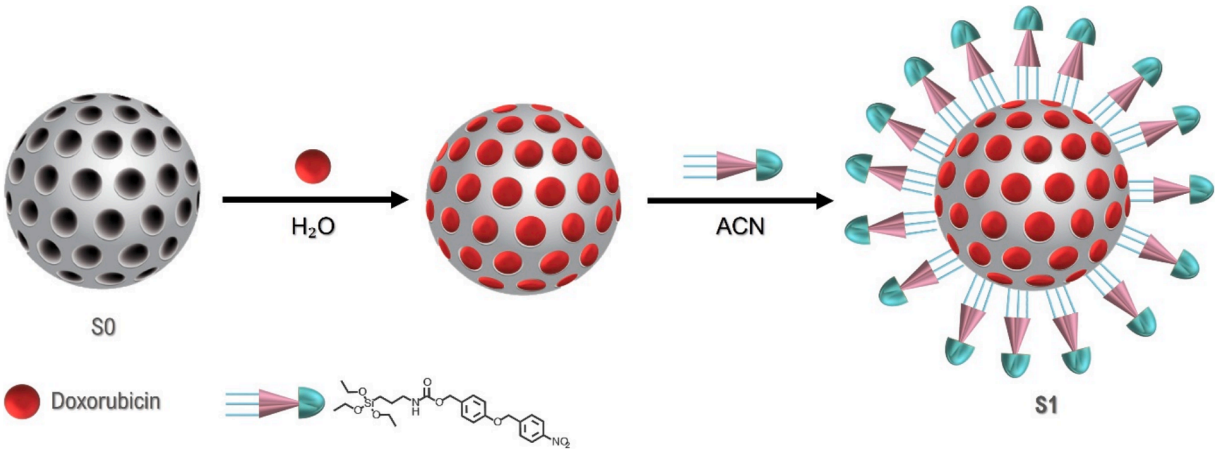

Fig. 2. Schematic representation of the synthesis of the **S1** nanomaterial.

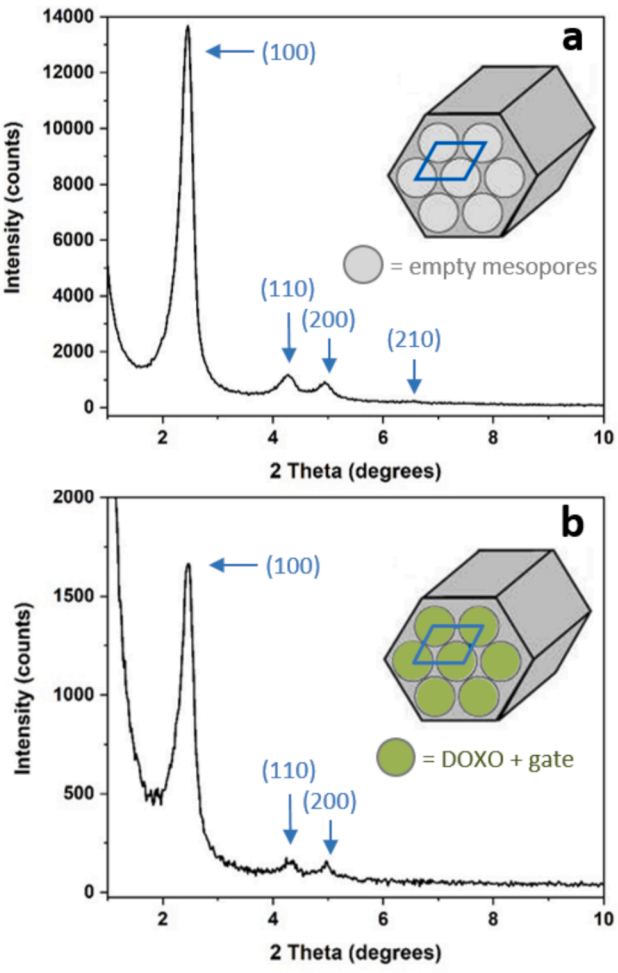

Fig. 3. PXRD patterns of (a) starting nanomaterial **S0**, and (b) final nanodevice **S1**.

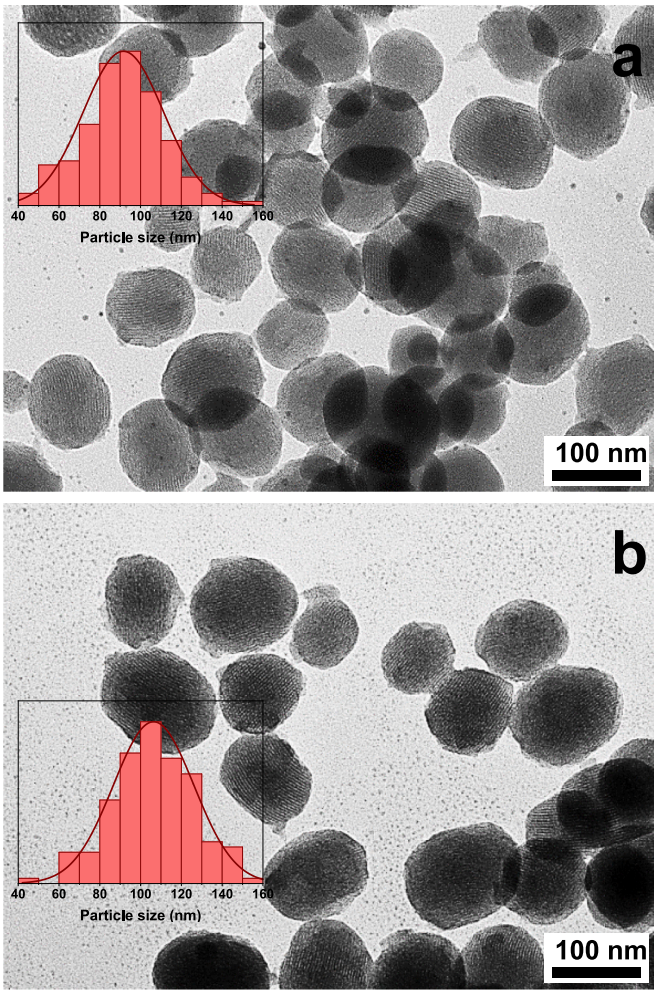

Fig. 4. TEM images of (a) solid **S0** and (b) nanodevice **S1**. The particle size distributions are presented in the insets.

development of a new hypoxia-responsive nanomaterial consisting of MSNs loaded with the drug doxorubicin (DOXO) and capped with a gatekeeper containing a self-immolative linker (Gavriel et al., 2022) attached to an aromatic nitro group. Reduction of the nitro moiety by nitroreductase enzymes induces a self-immolative elimination through an electronic cascade, leading to an irreversible disassembly of the gatekeeper that releases the cargo (Fig. 1). The nitroreductase-responsive gated MSNs are tested *in vitro* in A549 cells that are known to have a high NTR activity.

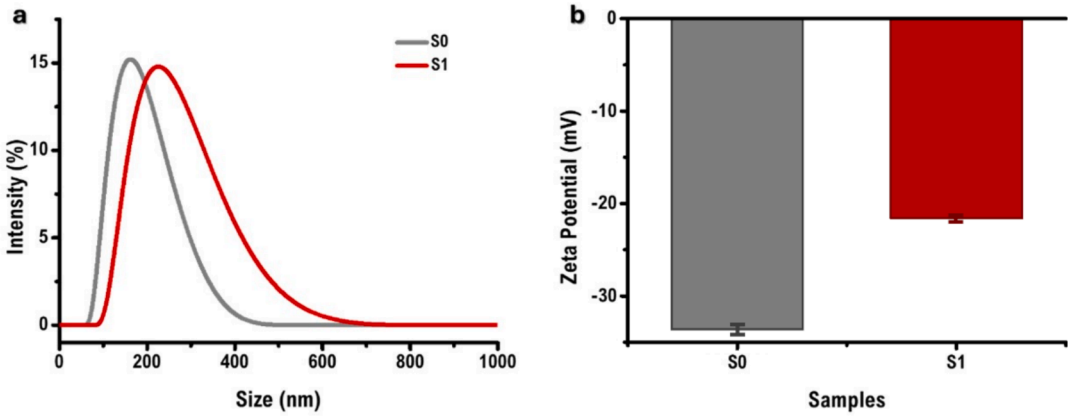

Fig. 5. (a) Hydrodynamic diameter distribution by DLS and (b) Zeta Potential for the starting MSNs **S0** and for nanodevice **S1**.

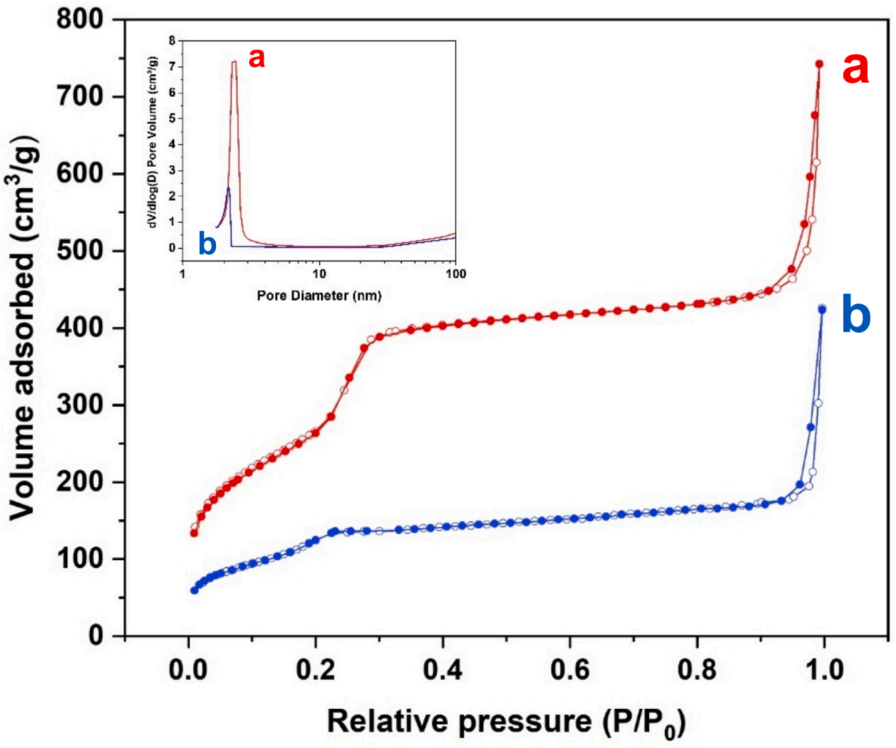

Fig. 6. N_2 adsorption–desorption isotherms for **(a) S0** nanoparticles and **(b)** nanodevice **S1**. The pore size distributions are shown in the inset.

2. Materials and methods

2.1. Chemicals and materials

The reagents employed in the synthesis were acquired from Sigma Aldrich (Darmstadt, Germany) and used without further purification. ^{1}H NMR and ^{13}C NMR spectra were registered with a Bruker Avance 300 MHz spectrophotometer (Billerica, MA, USA), referencing the shifts to the solvent peak. Fluorescence measures were carried out with a Shimadzu RF-6000 Spectrofluorometer (Nakagyo-ku, Kyoto, Japan), using a 10x2 mm path length cuvette. The synthesized solids were characterized by Powder X-ray diffraction (PXRD) carried out using a Bruker D8 Advance diffractometer with monochromatic Cu Kα source operated at 40 kV and 40 mA. Patterns were collected in steps of 0.02° (2θ) over the angular range 1–10.0° (2θ), with an acquisition time of 25 s per step. An electron microscopy study (HRTEM) was conducted with a JEOL JEM-1010 (Akishima, Tokyo, Japan) instrument operating at 100 kV. Nitrogen adsorption–desorption isotherms were recorded in an automated Micromeritics ASAP2020 instrument. Prior to the adsorption measurements, the samples were outgassed *in situ* in vacuum (10^{-6} Torr) at 75 °C for 15 h to remove adsorbed gases. Specific surface areas were calculated from the absorption data in the low-pressure range using the Brunauer–Emmett–Teller (BET) model. Pore size was determined following the BJH method. Dynamic light scattering (DLS) measurements were performed using Malvern Nanosizer ZS equipment (Malvern, UK). For MTT Assay, the absorbance was measured at 535 nm using a spectrophotometer VICTOR3^{TM} V 1420 (PerkinElmer, Finland).

2.2. Synthesis of (4-((4-nitrobenzyl)oxy)phenyl)methanol (2)

4-(Hydroxymethyl)phenol (**3**) (500 mg, 4.0 mmol) and K_2CO_3 (836 mg, 6.1 mmol) were dissolved in acetone (40 mL) under an argon atmosphere. 1-(Bromomethyl)-4-nitrobenzene (**4**) (871 mg, 4.0 mmol) was added, and the reaction mixture was refluxed for 5 h. After this time,

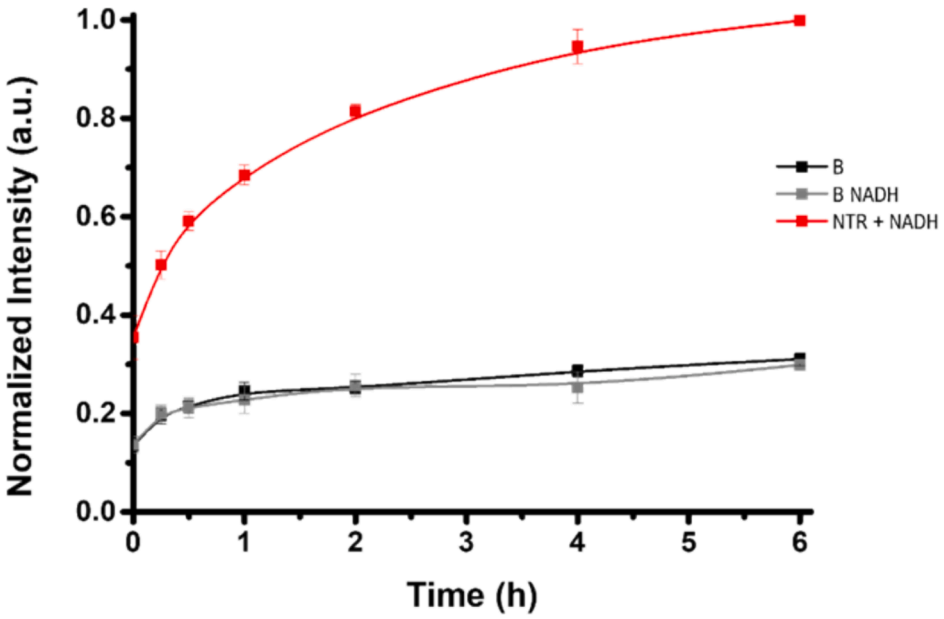

Fig. 7. DOXO release profiles from suspensions of **S1** in PBS buffer (pH = 7.4) in the absence and in the presence of NTR from *E. Coli* and NADH.

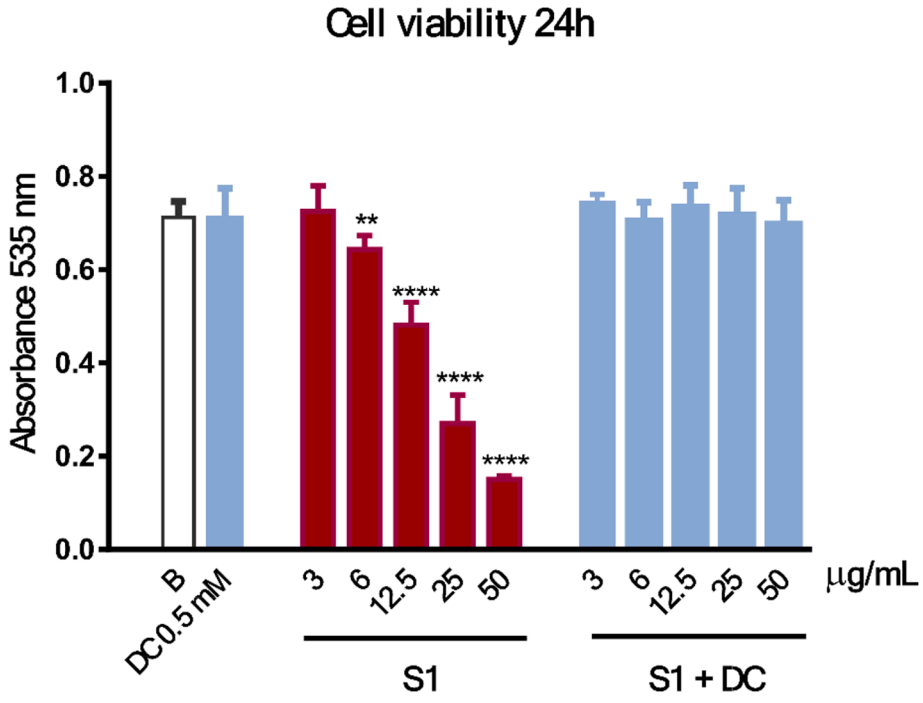

Fig. 8. MTT assay for A549 cell line viability after 24 h of treatment. Results are expressed as mean ± SD (n = 12). **p < 0.05, ****p < 0.0001 versus untreated cells (B). One-way ANOVA followed by Dunnet's test.

30 mL of H_2O were added to stop the reaction. Acetone was evaporated, and extraction was performed with ethyl acetate and water (3x 30 mL). The organic phase was dried with anhydrous $MgSO_4$, and the solvent was evaporated to give **2** as a pale yellow solid (921 mg, 88 %).

^{1}H NMR (300 MHz, $CDCl_3$): δ 8.25 (d, J = 9.0 Hz, 2H), 7.61 (d,J = 9.0 Hz, 2H), 7.32 (d, J = 8.7 Hz, 2H), 6.95 (d, J = 8.7 Hz, 2H), 5.18 (s, 2H), 4.64 (s, 2H) ppm.

^{13}C NMR (75 MHz, DMSO-d_6): δ 156.74, 146.95, 145.26, 135.20, 128.14, 128.14, 127.98, 127.98, 123.59, 123.59, 114.46, 67.96, 62.48 ppm.

*2.3. Synthesis of NTR-responsive molecular gate **NG1***

Compound **2** (259 mg, 1 mmol) was dissolved in toluene (10 mL) under an Argon atmosphere, and then dioctyl tin oxide (1 mmol%) was added. The solution was stirred for 10 min. Triethoxy(3-isocyanatopropyl)silane (**5**) (250 μL, 1 mmol) was added, and the reaction mixture was refluxed overnight. Toluene was evaporated to afford nitro gate **NG1** as pale-yellow oil (486 mg, 96 %).

^{1}H NMR (300 MHz, $CDCl_3$): δ 8.25 (d, J = 9.0 Hz, 2H), 7.60 (d, J = 9.0 Hz, 2H), 7.31 (d, J = 8.7 Hz, 2H), 6.94 (d, J = 8.7 Hz, 2H), 5.18 (s, 2H), 5.03 (s, 2H), 3.76 – 3.85 (m, 4H), 3.72 (q, J = 7.0 Hz, 2H), 3.18 (d, J = 6.3 Hz, 2H), 1.54 – 1.68 (m, 2H), 1.23 (dt, J = 8.6, 7.0 Hz, 9H), 0.58 –

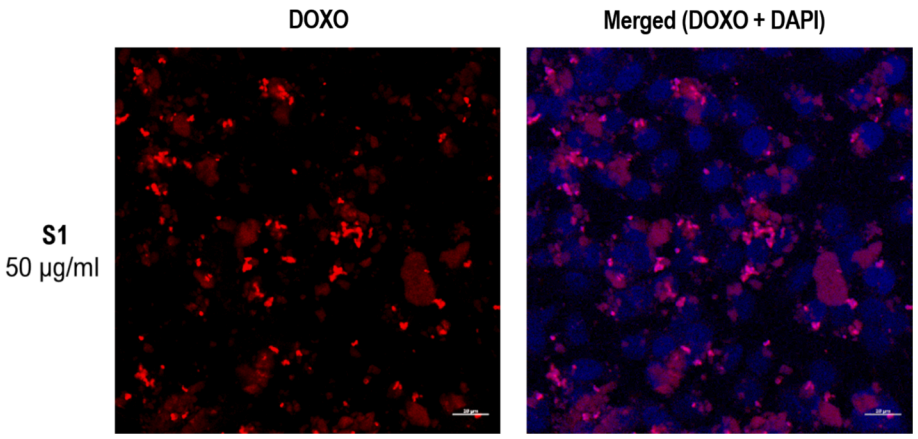

Fig. 9. Confocal imaging of A549 cells incubated with **S1** (50 µg/mL) during 4 h. Red chanel: DOXO fluorescence at 546 nm (l_{ex} = 470 nm). Blue fluorescence: DAPI stain cell nuclei. Pink stain: colocalization of DOXO within the nuclei. Representative image from three independent experiments. Scale bar = 20 µm.

0.64 (m, 2H) ppm.

^{13}C NMR (75 MHz, $CDCl_3$): δ 158.00, 147.60, 130.03, 129.88, 129.05, 128.76, 128.24, 127.58, 125.31, 123.85, 114.88, 114.79, 68.69, 64.88, 58.47, 29.71, 18.43, 18.28, 7.60 ppm.

HRMS: *m/z* calculated for $C_{24}H_{34}N_2O_8$ [M − NO_2 + Na]$^+$ 483.205, found 483.199.

2.4. Synthesis of mesoporous silica nanoparticles (MCM-41-type), *S0*

Cetyltrimethylammonium bromide (CTAB) (1.00 g, 2.74 mmol) was dissolved in 480 mL of deionized water by gentle stirring (150 rpm) before adding 3.5 mL of a 2 M NaOH solution until a pH of 8 was reached. The solution was heated to 80 °C, and when this temperature was reached, tetraethylorthosilicate (TEOS, 5.0 mL, 22.4 mmol) was added dropwise to the surfactant solution with maximum stirring, and a white suspension was observed. The mixture was stirred at 80 °C for 2 h. A white precipitate was obtained and isolated by centrifugation. After isolation, the solid was washed with deionized water until the pH of the solution was neutral, and the solid was dried at 70 °C overnight. To prepare the final **S0** material, the synthesized solid was calcined at 550 °C for 5 h under an oxidizing atmosphere to remove the surfactant residues.

2.5. Synthesis of *S1*

In a typical experiment, a mixture of **S0** (23 mg) and doxorubicin hydrochloride (DOXO, 10 mg) was suspended in ultrapure water (805 µL). The suspension was stirred overnight at room temperature. The suspension was then centrifugated, and the supernatant was removed. The DOXO-loaded MSNs were dried overnight at 37 °C. Then, the solid was resuspended in dry CH_3CN (805 µL), and **NG1** (70 mg) was added. The system was purged with Argon and stirred for 5 h at room temperature. After that, the suspension was centrifugated at 12,000 rpm for 5 min, **S1** was thoroughly washed with CH_3CN and water to remove the unencapsulated drug and the unattached gate, and then it was dried overnight at 37 °C.

2.6. Chemical reduction of the nitro compound *2* with sodium sulfide

Compound **2** (108 mg, 0.42 mmol) was dissolved in 10 mL of acetone and heated to reflux. A solution of Na_2CO_3 (89 mg, 0.84 mmol) and $Na_2S{\cdot}9H_2O$ (547 mg, 2.28 mmol) in 7 mL of distilled water was prepared and added dropwise to the solution of **2**. The mixture immediately turned dark brown and was stirred and refluxed for 24 h. The crude of the reaction mixture was extracted with $CHCl_3$ (3 x 20 mL), the organic phase was dried with anhydrous $MgSO_4$, and the solvent was evaporated to give a yellow oil.

2.7. Drug release studies from *S1* in solution

To study the release of the DOXO from the **S1** material, the biological hypoxic condition was generated with NTR and NADH, to induce the self-immolation of the nitro molecular gate **NG1**. Thus, 1 mg of solid **S1** was suspended in 1 mL of PBS buffer (pH = 7.4), and the suspension was separated into two 400 µL aliquots. After that, 60 µL of NTR (1 mg/mL) was added to the suspension in the presence and absence of NADH (50 mM). In the aliquot with NADH, 4 µL were added; in the other one, 4 µL of PBS buffer were added to the suspension to maintain a constant concentration. At the same time, 64 µL of PBS buffer were added to a blank aliquot. An aliquot containing only NADH was also prepared for a normoxic control (4 µL of NADH (50 mM) and 60 µL of PBS buffer). All suspensions were stirred at 37 °C, and the fluorescence of the DOXO (λ_{exc} = 480 nm, λ_{em} = 552 nm) was measured at predetermined intervals (0, 15 min, 30 min, 1 h, 2 h, 4 h, and 6 h). Aliquots were centrifuged (5 min at 12,000 rpm), measured, and returned to the original suspension.

2.8. Cell culture

A549 cells were cultured in Dulbecco's Modified Eagle Medium (DMEM) (Gibco^{TM}, Paisley, UK), supplemented with 10 % Fetal Bovine Serum (FBS), penicillin 100 U/mL and streptomycin 100 µg/mL (Gibco^{TM}, Paisley, UK) and maintained in a humidified incubator containing an atmosphere of 5 % CO_2 at 37 °C.

2.9. MTT assay

The MTT assay is a colorimetric test used to determine cell viability. The cellular succinate-dehydrogenase activity metabolizes the MTT, producing a violet-colored product whose absorbance intensity is directly proportional to cell viability. Experiments were carried out in A549 cells seeded in 96-well plates (Sarstedt®, Nümbrecht, Germany) at a concentration of 5x10^5 cells/mL (final volume 200 µL/well in DMEM 10 % FBS). After an overnight incubation to allow cell attachment, the medium was renewed (DMEM 1 % FBS). The cells were then incubated with 3, 6, 12.5, 25, and 50 µg/mL of **S1** for 24 h. In another set of experiments, cells were pretreated with dicoumarol (DC, 0.5 mM) for 60 min before the addition of **S1** to inhibit NTR activity.

After 24 h of incubation, the cells were washed with PBS (Gibco^{TM}, Paisley, UK), and a solution of 3-(4,5-dimethylthiazol-2-yl)-2,5-diphenyl tetrazole bromide (MTT, 200 µg/mL) (Sigma-Aldrich, St. Louis, Missouri, USA) in culture medium was added to incubate the cells for 1 h. The medium was then removed, and 100 µL of dimethylsulfoxide was

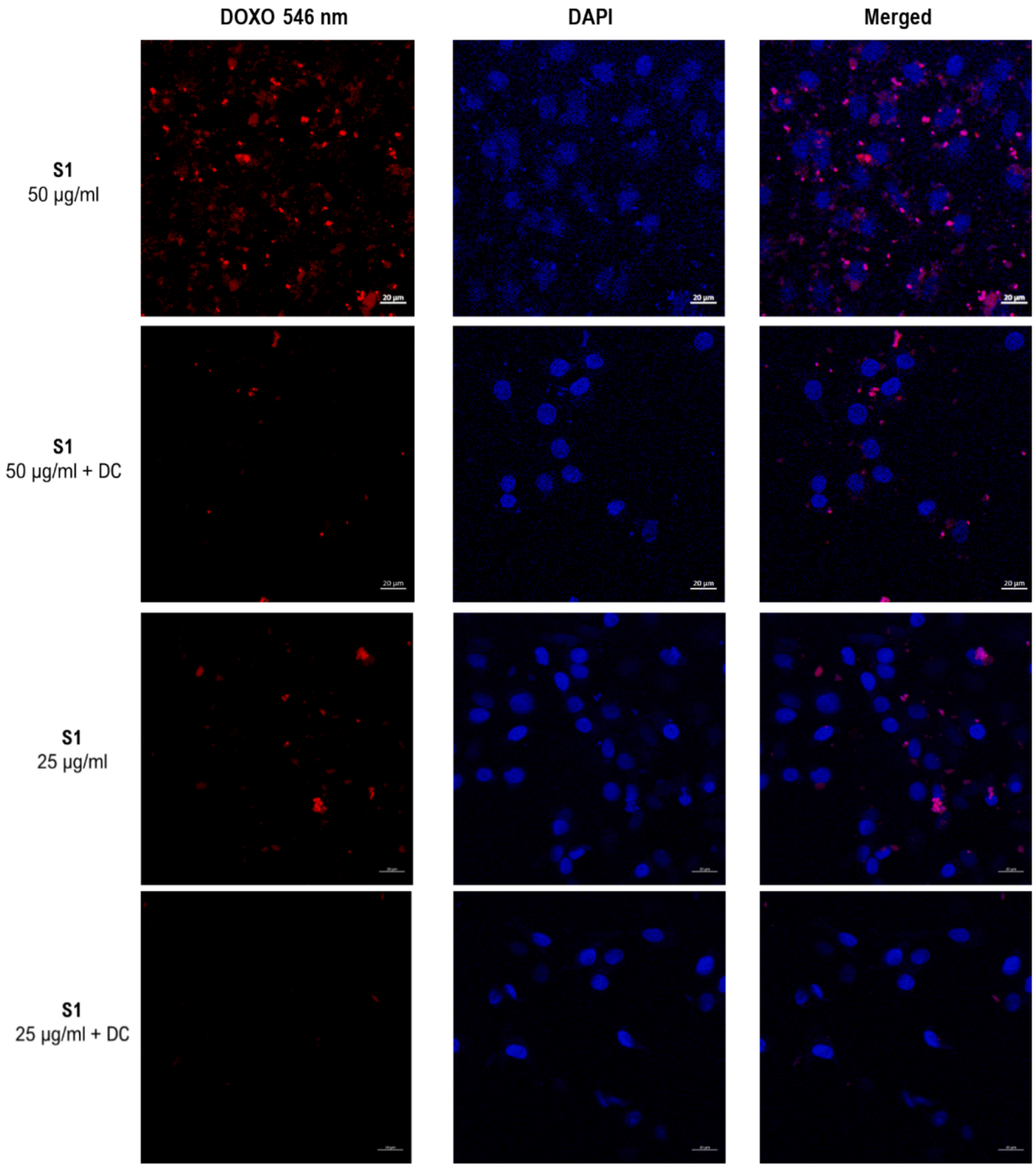

Fig. 10. Confocal imaging of A549 cells incubated with **S1** (25–50 µg/ml) during 4 h in the absence or presence of DC (0.5 mM). Red channel: DOXO fluorescence at 546 nm (λ_{ex} = 470 nm). Blue fluorescence: DAPI stain cell nuclei. Pink stain: colocalization of DOXO within the nuclei. Representative image from three independent experiments. Scale bar = 20 µm.

added to dissolve the formazan. The absorbance was measured at 535 nm using a spectrophotometer VICTOR3^{TM} V1420 (PerkinElmer, Finland).

Cell viability studies with THP-1 human monocytes: Similarly, THP-1 cells were cultured at 37 °C, 5 % CO2 in RPMI 1640 medium supplemented with 10 % SBF and 1 % penicillin/streptomycin. Differentiation of THP-1 to macrophages was performed seeding THP-1 in 96-well plates (5x105 cells/mL) and incubating them with 12-O-tetradecanoyl phorbol 13-acetate (TPA) 10 nM for three days. Then, adherent cells were washed with DMEM 1 % FBS and incubated with 3, 6, 12.5, 25, and 50 µg/mL of S1. After 24 h the cells were washed with PBS and MTT assay was performed as described before.

All the results are presented as the mean ± standard deviation (SD) of the values. The statistical treatment employed was the one-way ANOVA method, followed by Dunnet's multiple comparison test. This test creates confidence intervals between the means of different treatments and the untreated group.

Data analysis was performed using the GraphPad Prism 5 program (GraphPad Software, La Jolla, CA, USA). The symbol (*) indicates statistical significance compared to the untreated group.

2.10. Visualization of A549 cells by confocal microscopy imaging

A549 cells were seeded in a cell culture Chamber Slide^{TM} at a density of 5x10^4 cells per well in DMEM with 10 % FBS and incubated overnight to allow for cell attachment. The medium was then replaced with DMEM

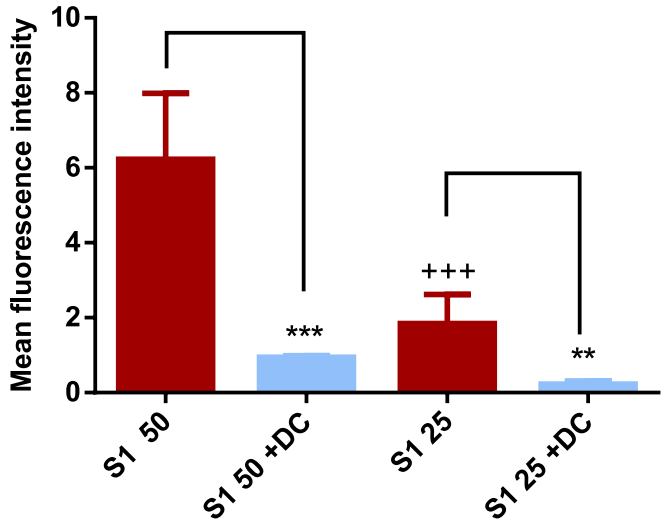

Fig. 11. Quantitative analysis of DOXO fluorescence intensity after confocal imaging in A549 incubated during 4 h with **S1** (25–50 μg/ml) in the absence or in the presence of DC (0.5 mM). Results are expressed as mean ± SD (n = 3). +++ $p < 0.001$ versus S1 (50 μg/mL). **$p < 0.01$, ***$p < 0.001$ versus de same concentration of S1 in absence of DC. One-way ANOVA followed by Dunnet's test.

containing 1 % FBS, and the cells were incubated with **S1** at concentrations of 25 and 50 μg/mL for 4 h. Prior to the addition of the material, some plates were pretreated with DC (0.5 mM) for 60 min. Finally, the cells were washed three times with PBS to remove unbound nanoparticles and fixed in 4 % *p*-formaldehyde. To visualize the nuclei, a drop of ProLong™ Gold Antifade Mountant mounting fluid with 4′,6-diamidino-2-phenylindole (DAPI, Molecular Probes™ Invitrogen, Paisley, UK) was added. The slide was observed in a Super-resolution Confocal Microscope LSM 980 (ZEISS LCS 980, Münster, Germany) with a 20X objective and Alexa 546 and DAPI channels. Quantification of images was carried out with the LSM 980 software.

3. Results and discussion

3.1. Design and synthesis of the nitroreductase-responsive molecular gate (*NG1*)

The gatekeeper **NG1** (Scheme 1), containing a terminal nitroaromatic group responsive to NTR, connected to a 4-hydroxybenzylalcohol self-immolative linker, was designed. To favor anchoring to the silica surface, **NG1** incorporates a trialcoxysilane moiety (R'-Si(OR)$_3$) with ethoxyl chains that are easily substituted by free silanol groups (Si-OH) in MSNs to form Si-O-Si covalent bonds. (Zheng et al., 2000) The triethoxysilane group is linked to the rest of the molecule trough a three-carbon aliphatic chain that provides flexibility to the gatekeeper. **NG1** is a self-immolative molecular gate in which a spontaneous fragmentation process is expected to be triggered after the reduction of the nitro group to amino by NTR as shown in Scheme 1. The reduction in size of the anchored molecule after hydrolysis by NTR is expected to induce DOXO release.

NG1 was synthesized in two steps, as shown in Scheme 2. In the first step, the phenolic –OH group in 4-(hydroxymethyl)phenol (**3**) is deprotonated by carbonate and acts as a nucleophile over 1-(bromomethyl)-4-nitrobenzene (**4**) to yield **2**. In the second step, the benzyl alcohol in **2** reacts with the isocyanate group of triethoxy(3-isocyanatopropyl)silane **5**, in the presence of dioctyltin oxide as a catalyst, to yield the NTR-responsive gatekeeper **NG1**. Compounds **2** and **NG1** were fully characterized by ^{1}H NMR, ^{13}C NMR, and MS.

3.2. Synthesis and characterization of the NTR-responsive nanodevice *S1*

MCM-41 type MSNs (**S0**) were synthesized *via* a sol–gel template method, using CTAB as a structure-directing agent and TEOS as a silica source, following previously reported procedures. (Cabrera et al., 2000; Radu et al., 2004) The pores of the MSNs were loaded with the drug DOXO and then the external surface was functionalized with **NG1** by reaction of the triethoxysilane groups of **NG1** with the silanol moieties on the silica surface, to yield nanomaterial **S1** (Fig. 2).

The starting synthesized MSNs (solid **S0**) and the final nanodevice **S1** were characterized following usual standard techniques such as TEM, PXRD, Zeta Potential, DLS, and N_2 adsorption/desorption isotherms. The PXRD pattern of **S0** (Fig. 3a) shows the four low-angle reflections typical of the hexagonal array, indexed as (100), (110), (200), and (210) Bragg peaks. The detection of up to four diffraction peaks is clearly indicative of the existence of highly ordered mesoporous silica. Compared to the starting material, the intensity of the peaks in **S1** decreased, the (110) and (200) reflections exhibit appreciable broadening, and the (210) peak is practically undetectable (Fig. 3b). The lower intensity of the peaks of the **S1** material is attributed to the loss of contrast caused by the filling of the pores with DOXO and the functionalization of the surface. Nevertheless, the detection of three diffraction peaks indicates the preservation of the order of the mesopore array after drug filling, and functionalization on the external surface.

Fig. 4 depicts the transmission electron microscopy (TEM) images of the starting MSNs **S0** and NTR-responsive nanocarrier **S1**. MSNs exhibit a particle size of 92 ± 20 nm (Fig. 5a). Their morphology is predominantly spherical, with a minor population of particles exhibiting slight elongation along the mesopore direction (00 l). All particles exhibit ordered patterns comprising alternating light and dark spots arranged in stripes. These patterns can be associated with the mesopores and pore walls, respectively. Therefore, the preferential orientation of the MSNs demonstrates the existence of ordered cylindrical mesopores and can be described as exhibiting a hexagonal organization, in agreement with the aforementioned XRD data. The morphology and degree of order are preserved after DOXO loading and gate incorporation (Fig. 5b). The particles are observed to be spherical or slightly elongated in shape, with an average diameter of 106 ± 20 nm. The orientation of the mesopores in **S1** is indistinguishable from that observed for the initial MSNs **S0**.

The DLS curves (Fig. 5a) show an average hydrodynamic diameter value of 156.0 ± 0.9 nm and 228.9 ± 0.6 nm for the starting MSNs (**S0**) and **S1**, respectively. In both cases, a hydrodynamic radius greater than the particle size obtained by TEM was observed as we expected. The zeta potential exhibits values of –33.6 ± 1.1 mV and –21.6 ± 0.4 mV for the starting MSNs and **S1**, respectively (Fig. 5b). The observed reduction in zeta potential upon incorporation of the **NG1** gatekeeper can be attributed to the reaction of **NG1** with the silanol groups that reduces the amount of Si-O$^-$ groups in the surface of the silica nanoparticles, further supporting the functionalization process.

N_2 adsorption–desorption (Fig. 6) studies on the starting MSNs **S0** show a type IV isotherm, typical of mesoporous materials according to the IUPAC classification, with no hysteresis cycle, and the shape of the curve suggests the existence of uniform and cylindrical mesopores with a pore diameter of 2.36 ± 0.07 nm and a total pore volume of 0.74 ± 0.03 cm^3/g, both calculated by using the BJH model on the adsorption branch of the isotherm. Also, the application of the BET model results in a value for the total specific surface of 971.7 ± 0.7 m^2/g for **S0**. After the functionalization of the material, the N_2 adsorption–desorption isotherm curve of **S1** is typical of mesoporous systems with partially filled mesopores, for which BET and BJH models indicated a reduction of the specific surface to 334.6 ± 0.8 m^2/g and a decrease of pore volume and size to 0.12 ± 0.04 cm^3/g and 2.0 ± 0.2 nm, respectively. These changes after loading and functionalization are also reflected in the pore size distributions (inset of Fig. 6). The significant decrease in pore volume and size associated with mesopores indicates that drug incorporation and gate functionalization has largely blocked the pore

system. Considering the decrease in mesopore BJH volume, it was calculated that 84 % of the pores have been loaded with DOXO and functionalized with the **NG1** gatekeeper. Additionally, both samples present a similar textural porosity linked to the voids between particles (0.44 ± 0.04 and 0.32 ± 0.05 cm^3/g for samples **S0** and **S1**, respectively).

Thermogravimetric (TGA) (Fig. S6) and elemental analysis (EA) were also performed to calculate the amount of gatekeeper **NG1** and DOXO in **S1**. From TGA and EA measurements, contents of 0.46 mmol/g for **NG1** and 0.08 mmol/g for DOXO in **S1** were determined.

3.3. Controlled release experiments in solution, in the presence of NTR and NADH

First, the self-immolation of the molecular gate was tested using a chemical reductant, by reducing the nitro group in **2** with sodium sulfide in acetone-H_2O. The TLC analysis of the crude showed the disappearance of the starting molecule and the presence of two new products. The immolative reaction was also followed by ^1H NMR that unequivocally confirmed the presence of peaks corresponding phenol and aniline derivatives (see Scheme 1).

Then, the response of **S1** to NTR and NADH, simulating a hypoxic environment, was tested. NTR from *E. coli* and NADH were used for this purpose. These studies were carried out in PBS buffer pH = 7.4, by measuring the fluorescence emission of DOXO at 552 nm (λ_{exc} = 480 nm) with time, and assuming a linear relationship between the maximum emission intensity and the amount of DOXO released. Fig. 7 shows the DOXO release profile in the abscence of any reductants (blank, B), in the presence of NADH and in the presence of NADH + NTR. As can be observed in the Figure, very low cargo release was observed after 6 h of incubation of **S1** or **S1** + NADH in PBS. On the other hand, in the presence of NADH and NTR, a remarkable payload release was observed after 30 min, reaching the maximum amount of DOXO release after 6 h. This behavior agrees with the previously described enzymatic reduction and self-immolation of the molecular gate allowing delivery of the entrapped drug.

To determine the maximum amount of DOXO that can be released from the **S1** material, a forced delivery of the cargo in the presence of DMSO was carried out. For this, the material was incubated with NTR + NADH for 24 h to ensure the greatest possible reduction in the nitro gate and to ensure the highest possible gate opening. After centrifugation, the supernatant was removed and measured by fluorescence. Then, DMSO was added to the material, to deliver as much DOXO as possible and the suspension was incubated for 2 h. After centrifugation, the supernatant was removed, and its fluorescence emission was measured again. The total concentration of DOXO delivered from **S1** was calculated as 20 mg/g, which represents ca. 50 % of the total load.

3.4. In vitro drug release studies in cells

3.4.1. Cell viability studies

In Vitro cytotoxicity studies with **S1** were undertaken. The A549 cell line was selected considering its high NTR activity. (Chevalier et al., 2016) Moreover, the studies were carried out in the presence and absence of dicoumarol (DC), which is well known NTR inhibitor. (Johansson et al., 2003) First, cell viability studies in the presence of **S1**, with and without DC, were performed after 24 h by MTT assay (Fig. 8). (Borenfreund et al., 1988) **S1** induced a concentration-dependent decrease of cell viability, whereas similar experiments in the presence of the NTR inhibitor DC did no induce cell death. This agrees with the mechanism outlined above; the presence of NTR in A549 cells induce gate opening in **S1** and delivery of the DOXO cargo, whereas this is not observed in the presence of the DC inhibitor. In addition, it was confirmed that DC has no effect on cell viability at the assayed concentration (0.5 mM). Finally, the same concentration-dependent study was performed in THP-1 human monocytes, used as a control cell line with low expression of nitroreductase. (Herrlinger et al., 2020) As shown in Fig. S7, treatment with **S1** did not significantly affect cell viability at none of the concentrations tested, demonstrating that the gate remains closed in cell types with low NTR activity.

3.4.2. Confocal microscopy imaging

Internalization and DOXO delivery from **S1** in A549 cells were also studied by confocal microscopy. DAPI was used as a blue-fluorescent nuclear counterstain. As shown in Fig. 9, the red fluorescence of DOXO released by **S1** was primarily distributed within the cell nuclei, while **S1** was localized around it (merged image).

In another set of experiments, **S1** (25–50 μg/mL) was incubated in the absence or the presence of DC. As shown in Fig. 10, there was a concentration-dependent red fluorescence when A549 was incubated with **S1.** In both cases, the intensity of fluorescence was clearly reduced in the presence of DC. These results were confirmed by quantitative analysis of images, which showed a significant reduction of DOXO fluorescence after incubation with **S1** at lower dose, but, above all, after preincubation of the cells with DC (Fig. 11).

4. Conclusions

A new hybrid organic–inorganic nanomaterial **S1**, incorporating the anticancer drug doxorubicin (DOXO) and capped with a NTR-responsive molecular gate was synthesized and fully characterized. This gated nanocarrier consists of MCM-41-type MSNs particles functionalized with the gatekeeper **NG1**, which contains a self-immolative linker attached to an aromatic nitro group. This molecular gate keeps the DOXO inside the porous material. However, in the presence of NTR and NADH, the molecular gate undergoes a self-immolative process, triggered by the reduction of the terminal aromatic nitro group to amine, causing the release of DOXO from inside the pores of the nanocarrier. Additionally, studies with the A549 cell line, which is known to present high NTR activity, were conducted. In the presence of DC, an inhibitor of NTR, the material was non-toxic to cells. However, without DC, cell viability clearly decreased in the presence of **S1**, which means that the DOXO was released due to the gate opening in the presence of the NTR from the cellular media. Fluorescence emission microscopy experiments with A549 cells and **S1**, in both, the presence and absence of DC, showed a reduction in fluorescence intensity in the presence of DC. Finally, the absence of **S1** cytotoxicity in THP-1 monocytic cells (with low NTR activity) also confirms that the nitro gate **NG1** opens selectively in response to NTR.

CRediT authorship contribution statement

Mariana Barros: Writing – original draft, Investigation, Data curation. **José A. Sáez:** Writing – original draft, Validation, Formal analysis. **Pau Arroyo:** Writing – original draft, Formal analysis. **J. Vicente Ros-Lis:** Funding acquisition, Formal analysis, Data curation. **M. Dolores Garrido:** Data curation. **Ramón Martínez-Máñez:** Writing – review & editing, Validation, Funding acquisition. **M. Carmen Terencio:** Writing – original draft, Validation, Methodology, Formal analysis. **M. Carmen Montesinos:** Writing – review & editing, Validation, Formal analysis. **Pablo Gaviña:** Writing – review & editing, Supervision, Methodology, Funding acquisition, Conceptualization.

Declaration of competing interest

The authors declare that they have no known competing financial interests or personal relationships that could have appeared to influence the work reported in this paper.

Acknowledgements

We thank the Spanish Government for grants PID2021-126304OB-

C41, PID2021-126304OB-C42, and PID2021-126304OB-C43, funded by MCIN/ AEI/10.13039/501100011033/ and by European Regional Development Fund - A way of making Europe, EU. We also acknowledge the Generalitat Valenciana (Conselleria de Educación, Universidades y Empleo) for grants CIAICO/2022/146 and CIPROM/2021/007. SCSIE (Universidad de Valencia) is gratefully acknowledged for all the equipment employed. NMR spectra were registered at the U26 facility of ICTS "NAMBIOSIS" at the Universitat de València.

Appendix A. Supplementary material

Supplementary data to this article can be found online at https://doi.org/10.1016/j.ijpharm.2025.125326.

Data availability

No data was used for the research described in the article.

References

Aznar, E., Oroval, M., Pascual, L., Murguía, J.R., Martínez-Máñez, R., Sancenón, F., 2016. Gated materials for on-command release of guest molecules. Chem. Rev. 116, 561–718. https://doi.org/10.1021/acs.chemrev.5b00456.

Borenfreund, E., Babich, H., Martin-Alguacil, N., 1988. Comparisons of two in vitro cytotoxicity assays-the neutral red (NR) and tetrazolium MTT tests. Toxicol. Vitro 2, 1–6. https://doi.org/10.1016/0887-2333(88)90030-6.

Cabrera, S., El Haskouri, J., Guillem, C., Latorre, J., Beltrán-Porter, A., Beltrán-Porter, D., Marcos, M.D., Amorós, P., 2000. Generalised syntheses of ordered mesoporous oxides: the atrane route. Solid State Sci. 2, 405–420. https://doi.org/10.1016/S1293-2558(00)00152-7.

Cancer Tomorrow. International Agency for Research on Cancer, WHO. https://gco.iarc.fr/tomorrow/en/dataviz/isotype?types=0&single_unit=500000&mode=population&group_populations=1&multiple_cancers=0&cancers=39&multiple_populations=1 (accessed 2023-11-12).

Chevalier, A., Zhang, Y., Khdour, O.M., Kaye, J.B., Hecht, S.M., 2016. Mitochondrial nitroreductase activity enables selective imaging and therapeutic targeting. J. Am. Chem. Soc. 138, 12009–12012. https://doi.org/10.1021/JACS.6B06229.

Debela, D. T., Muzazu, S. G. Y., Heraro, K. D., Ndalama, M. T., Mesele, B. W., Haile, D. C., Kitui, S. K., Manyazewal, T. New Approaches and Procedures for Cancer Treatment: Current Perspectives. *SAGE Open Med.* **2021**, 9. https://doi.org/10.1177/20503121211034366.

Elmes, R.B.P., 2016. Bioreductive fluorescent imaging agents: applications to tumour hypoxia. Chem. Commun. 52, 8935. https://doi.org/10.1039/c6cc01037g.

Fang, Y., Shi, W., Hu, Y., Li, X., Ma, H., 2018. A dual-function fluorescent probe for monitoring the degrees of hypoxia in living cells via the imaging of nitroreductase and adenosine triphosphate. Chem. Comm. 54, 5454–5457. https://doi.org/10.1039/C8CC02209G.

Gavriel, A.G., Sambrook, M.R., Russell, A.T., Hayes, W., 2022. Recent advances in self-immolative linkers and their applications in polymeric reporting systems. Polym. Chem. 13, 3188–3269. https://doi.org/10.1039/d2py00414c.

Graham, K., Unger, E. Overcoming tumor hypoxia as a barrier to radiotherapy, chemotherapy and immunotherapy in cancer treatment. *Int. J. Nanomed.* **2018**, 6049-6058.

Herrlinger, E.-M., Hau, M., Redhaber, D.M., Greve, G., Willmann, D., Steimle, S., Müller, M., Lübbert, M., Miething, C.C., Schüle, R., Jung, M., 2020. Nitroreductase-mediated release of inhibitors of lysine-specific demethylase 1 (LSD1) from prodrugs in transfected acute myeloid leukaemia cells. ChemBiochem 21, 2329–2347. https://doi.org/10.1002/cbic.202000138.

Hompland, T., Fjeldbo, C.S., Lyng, H., 2021. Tumor hypoxia as a barrier in cancer therapy: why levels matter. Cancers 13, 499. https://doi.org/10.3390/CANCERS13030499.

Johansson, E., Parkinson, G.N., Denny, W.A., Neidle, S., 2003. Studies on the nitroreductase prodrug-activating system. Crystal structures of complexes with the inhibitor dicoumarol and dinitrobenzamide prodrugs and of the enzyme active form. J. Med. Chem. 46, 4009–4020. https://doi.org/10.1021/JM030843B.

Khatoon, S., Han, H.S., Jeon, J., Rao, N.V., Jeong, D.-W., Ikram, M., Yasin, T., Yi, G.-R., Park, J.H., 2018. Hypoxia-responsive mesoporous nanoparticles for doxorubicin delivery. Polymers 10, 390. https://doi.org/10.3390/polym10040390.

Kumari, R., Sunil, D., Ningthoujam, R.S., 2020. Hypoxia-responsive nanoparticle-based drug delivery systems in cancer therapy: an up-to-date review. J. Control. Release 319, 135–156. https://doi.org/10.1016/J.JCONREL.2019.12.041.

Lee, J., Oh, E.-T., Yoon, H., Kim, C.W., Han, Y., Song, J., Jang, H., Park, H.J., Kim, C., 2017. Mesoporous nanocarriers with a stimulus-responsive cyclodextrin gatekeeper for targeting tumor hypoxia. Nanoscale 9, 6901. https://doi.org/10.1039/c7nr00808b.

Li, Y., Jeon, J., Park, J.H., 2020. Hypoxia-responsive nanoparticles for tumor-targeted drug delivery. Cancer Lett. 490, 31–43. https://doi.org/10.1016/j.canlet.2020.05.032.

Minassian, L.M., Cotechini, T., Huitema, E., Graham, C.H., 2019. Hypoxia-induced resistance to chemotherapy in cancer. Adv. Exp. Med. Biol. 1136, 123–139. https://doi.org/10.1007/978-3-030-12734-3_9.

Mousa, S.A., Bharali, D.J., 2011. Nanotechnology-based detection and targeted therapy in cancer: nano-bio paradigms and applications. Cancers 3, 2888–2903. https://doi.org/10.3390/cancers3032888.

Ng, L., Navarro, A., Law, W.L., 2023. Evolving roles of PiRNAs in solid tumors (Editorial). Front. Oncol. 13, 1178634. https://doi.org/10.3389/fonc.2023.1178634.

Radu, D.R., Lai, C.Y., Jeftinija, K., Rowe, E.W., Jeftinija, S., Lin, V.S.Y., 2004. Polyamidoamine dendrimer-capped mesoporous silica nanosphere-based gene transfection reagent. J. Am. Chem. Soc. 126, 13216–13217. https://doi.org/10.1021/JA046275M.

Siemann, D.W., Horsman, M.R., 2015. Modulation of the tumor vasculature and oxygenation to improve therapy. Pharmacol. Ther. 153, 107–124. https://doi.org/10.1016/j.pharmthera.2015.06.006.

Sørensen, B.S., Horsman, M.R., 2020. Tumor hypoxia: Impact on radiation therapy and molecular pathways. Front. Oncol. 10, 526362. https://doi.org/10.3389/FONC.2020.00562.

Thambi, T., Deepagan, V.G., Yoon, H.Y., Han, H.S., Kim, S.H., Son, S., Jo, D.G., Ahn, C. H., Suh, Y.D., Kim, K., Kwon, I.C., Lee, D.S., Park, J.H., 2014. Hypoxia-responsive polymeric nanoparticles for tumor-targeted drug delivery. Biomaterials 35, 1735–1743. https://doi.org/10.1016/J.BIOMATERIALS.2013.11.022.

Vaupel, P., Mayer, A., 2007. Hypoxia in cancer: significance and impact on clinical outcome. Cancer Metastasis Rev. 26, 225–239. https://doi.org/10.1007/s10555-007-9055-1.

Wang, K., Lu, J., Li, J., Gao, Y., Mao, Y., Zhao, Q., Wang, S., 2021. Current trends in smart mesoporous silica-based nanovehicles for photoactivated cancer therapy. J. Control. Release 339, 445–472. https://doi.org/10.1016/j.jconrel.2021.10.005.

Xu, Q., Yang, Y.Y., Lu, J., Lin, Y., Feng, S., Luo, X., Di, D., Wang, S., Zhao, Q., 2022. Recent trends of mesoporous silica-based nanoplatforms for nanodynamic therapies. Coord. Chem. Rev. 21, 214687. https://doi.org/10.1016/j.ccr.2022.214687.

Yan, Q., Guo, X., Huang, X., Meng, X., Liu, F., Dai, P., Wang, Z., Zhao, Y., 2019. Gated mesoporous silica nanocarriers for hypoxia-responsive cargo release. ACS Appl. Mater. Interfaces 11, 24377–24385. https://doi.org/10.1021/acsami.9b04142.

Ye, M., Zhang, W., Xu, H., Xie, P., Song, L., Sun, X., Li, Y., Wang, S., Zhao, Q., 2025. Fe-doped biodegradable dendritic mesoporous silica nanoparticles for starvation therapy and photothermal-enhanced cascade catalysis in tumor therapy. J. Colloid Interface Sci. 678, 378–392. https://doi.org/10.1016/j.jcis.2024.08.172.

Zdrowowicz, M., Spisz, P., Hać, A., Herman-Antosiewicz, A., Rak, J., 2022. Influence of hypoxia on radiosensitization of cancer cells by 5-bromo-2′-deoxyuridine. Int. J. Mol. Sci. 23, 1429. https://doi.org/10.3390/IJMS23031429.

Zheng, S., Gao, L., Guo, J., 2000. Synthesis and characterization of functionalized MCM-41 with copper– and manganese–phenanthroline complexes. J. Solid State Chem. 152, 447–452. https://doi.org/10.1006/JSSC.2000.8708.

Zhou, H., Qin, F., Chen, C., 2020. Designing hypoxia-responsive nanotheranostic agents for tumor imaging and therapy. Adv. Health. Mater. 10, 2001277. https://doi.org/10.1002/adhm.202001277.